# Numerical Simulation of the Towing Tank Problem Using High Order Schemes

**L. Beneš, J. Fürst, and Ph. Fraunié**

**Abstract** The article deals with the numerical simulation of 2D and 3D unsteady incompressible flows with stratifications. The mathematical model is based on the Boussinesq approximation of the Navier–Stokes equations. The flow field in the towing tank with a moving sphere is modelled for a wide range of Richardson numbers. The obstacle is modeled via appropriate source terms. The resulting set of partial differential equations is then solved by the fifth-order finite difference WENO scheme, or by the second-order finite volume AUSM MUSCL scheme. For the time integration, the second-order BDF method was used. Both schemes are combined with the artificial compressibility method in dual time.

## 1 Introduction

Modelling of Atmospheric Boundary Layer (ABL) flows plays a significant role in many industrial applications. It is well known that the influence of the stratification is significant in many processes in ABL flows (e.g., it affects the transport of pollutants, plays a significant role in determining the environmental and human consequences of accidents). Stratified flows in environmental applications are characterized by a variation of fluid density in the vertical direction that can result in qualitative and quantitative changes of the flow by buoyancy. Stable stratification generally suppresses any vertical mixing of mass and momentum. The present work was motivated by a desire to obtain a better understanding of these effects.

L. Beneš (✉)
Department of Technical Mathematics, Faculty of Mechanical Engineering,
Czech Technical University in Prague, Karlovo náměstí 13, 12135 Praha 2, Czech Republic,
E-mail: benes@marian.fsik.cvut.cz

A.F. Hegarty et al. (eds.), *BAIL 2008 - Boundary and Interior Layers.*
Lecture Notes in Computational Science and Engineering,
DOI: 10.1007/978-3-642-00605-0, 

## 2 Mathematical Model

The flow in ABL can be usually assumed to be incompressible. Nevertheless, the density is not constant owing to temperature changes, gravity, etc. Thus an equation for the density must be considered. This type of flow is described by the Navier–Stokes equations for viscous incompressible flow with variable density; these equations are simplified by the Boussinesq approximation. Density and pressure are divided into two parts: a background part (with subscript $_0$) plus a perturbation (with superscript $'$). The background component is chosen to fulfill the hydrostatic balance equation $\partial p_0(z)/\partial z = -\rho_0(z)g$. The system of equations obtained is partly linearized around the average state $\rho_*$. The resulting set of equations can be written in the form

$$\begin{aligned} \frac{D\rho'}{Dt} &= -w\frac{d\rho_0}{dz}, \\ \frac{D\mathbf{u}}{Dt} + \frac{1}{\rho_*}\nabla p' &= \nu\Delta\mathbf{u} + \frac{\rho'}{\rho_*}\mathbf{g} + \frac{1}{\rho_*}\mathbf{f}, \\ \nabla\mathbf{u} &= 0, \end{aligned} \tag{1}$$

where $\rho$ is the density, $\mathbf{u} = (u, v, w)$ is the velocity, $p$ is the pressure, $\nu$ is the viscosity, $\mathbf{g} = (0, 0, -g)$ is the gravity and $\mathbf{f}$ represents other forces (e.g., Coriolis force, source terms). We assume that $\rho_* = 1$ and we shall omit the primes above the density and pressure disturbances.

Equations (1) are rewritten in the vector conservative form

$$P W_t + F(W)_x + G(W)_y + H(W)_z = S(W).$$

Here $W = [\rho, u, v, w, p]^T$, $F = F^{in} - \nu F^v$, $G = G^{in} - \nu G^v$ and $H = H^{in} - \nu H^v$ contain the inviscid fluxes $F^{in}$, $G^{in}$, $H^{in}$ and viscous fluxes $F^v$, $G^v$, $H^v$, while $S$ is the gravity and source term and $P = diag(1, 1, 1, 1, 0)$. These fluxes and source term are

$$\begin{aligned} F^{in}(W) &= [\rho u, u^2 + p, uv, uw, u]^T, & G^{in}(W) &= [\rho v, uv, v^2 + p, vw, v]^T, \\ H^{in}(W) &= [\rho w, uw, vw, w^2 + p, w]^T, & S(W) &= [-v d\rho_0/dz, 0, 0, -\rho g, 0]^T \end{aligned} \tag{2}$$

$$\begin{aligned} F^v(W) &= [0, u_x, v_x, w_x, 0]^T, & G^v(W) &= [0, u_y, v_y, w_y, 0]^T, \\ H^v(W) &= [0, u_z, v_z, w_z, 0]^T. \end{aligned}$$

# 3 Numerical Schemes

## *3.1 Spatial Discretization*

Two different numerical schemes were used for the spatial discretization. We discretize only terms containing spatial derivatives. The system of ordinary differential equations (with respect to the time derivative) that is generated is solved by an appropriate ODE method; see [Bla01].

The first scheme is based on a flux-splitting method for incompressible flow and WENO-interpolation. The second method is the finite volume AUSM MUSCL scheme with the Hemker–Koren limiter.

### 3.1.1 Flux Splitting for Incompressible Flows

The discretization in space is achieved by standard fourth-order differences for viscous terms and by the following high-order flux-splitting method [Issa85]. Divide the inviscid flux $F^{in}(W)$ into two parts, the convective flux $F^c(W) = [\rho u, u^2, uv, uw, 0]^T$ and the pressure flux $F^p(W) = [0, p, 0, 0, \beta^2 u]^T$, then approximate the flux derivative by

$$F^{in}(W)_x\big|_i \approx \frac{1}{\Delta x}\left[F^c_{i+1/2} - F^c_{i-1/2}\right] + \frac{1}{\Delta x}\left[F^p_{i+1/2} - F^p_{i-1/2}\right]. \tag{3}$$

Here each subscript denotes the value at the corresponding point on the Cartesian grid (or, in the AUSM case, the mean value over the corresponding finite volume). For simplification of the next text, only the spatial index $i$ in the $x-$ direction is preserved; the remaining two indexes are omitted. The high-order weighted ENO scheme [Jiang96] is chosen as the interpolation method. The original WENO interpolation uses an upwind bias and it can be formally written in the following form (function `weno5` is described in [Jiang96]):

$$\phi_{i+1/2} = \begin{cases} \phi^+_{i+1/2} = \texttt{weno5}(\phi_{i-2}, \phi_{i-1}, \phi_i, \phi_{i+1}, \phi_{i+2}) & \text{if } u_{i+1/2} > 0, \\ \phi^-_{i+1/2} = \texttt{weno5}(\phi_{i+3}, \phi_{i+2}, \phi_{i+1}, \phi_i, \phi_{i-1}) & \text{if } u_{i+1/2} \le 0. \end{cases} \tag{4}$$

It is still necessary to determine the velocity $u_{i+1/2}$.

This interpolation is applied to the incompressible case separately for the convective and pressure terms. In agreement with mathematical analysis the convective part is discretized by simple upwinding, the third component of the pressure is approximated by backward differencing and the fourth component by a forward difference. The final scheme takes the form

$$u_{i+1/2} := (u^+_{i+1/2} + u^-_{i+1/2})/2,\, p_{i+1/2} := (p^+_{i+1/2} + p^-_{i+1/2})/2, \tag{5}$$

$$F^c(W)_{i+1/2} := \begin{bmatrix} (\rho u)^{\pm}_{i+1/2} \\ (u^2)^{\pm}_{i+1/2} \\ (uv)^{\pm}_{i+1/2} \\ (uw)^{\pm}_{i+1/2} \\ 0 \end{bmatrix}, \quad F^p(W) := \begin{bmatrix} 0 \\ p_{i+1/2} + \beta \frac{u^+_{i+1/2} - u^-_{i+1/2}}{2} \\ 0 \\ 0 \\ u_{i+1/2} + \frac{p^+_{i+1/2} - p^-_{i+1/2}}{2\beta} \end{bmatrix}, \tag{6}$$

where + or − is taken in the convective flux according to the sign of $u_{i+1/2}$.

A similar algorithm is applied in other directions for the fluxes $G$, $H$. The resulting scheme has high-order accuracy in space. It was validated for the case of compressible inviscid flows by a computation of shock-vortex interaction; see [Furst96].

### 3.1.2 AUSM Scheme

The finite volume AUSM scheme was used for spatial discretization of the inviscid fluxes in our second scheme. Until now we have applied it only in the 2D case but an extension to 3D is being prepared.

$$\begin{aligned} \int_\Omega (F^{in}_x + G^{in}_y) dS &= \oint_{\partial\Omega} (F^{in} n_x + G^{in} n_y) dl \\ &\approx \sum_{k=1}^{4} \left[ u_n \begin{pmatrix} \varrho \\ u \\ v \\ \beta^2 \end{pmatrix}_{L/R} + p \begin{pmatrix} 0 \\ n_x \\ n_y \\ 0 \end{pmatrix} \right] \Delta l_k \end{aligned} \tag{7}$$

where $n$ is the normal vector, $u_n$ the normal velocity vector, and $(q)_{L/R}$ are quantities on the left/right hand side of the face. These quantities are computed using MUSCL reconstruction with the Hemker–Koren limiter:

$$q_R = q_{i+1} - \frac{1}{2}\delta_R, \quad q_L = q_i + \frac{1}{2}\delta_L,$$

$$\delta_{L/R} = \frac{a_{L/R}(b^2_{L/R} + 2) + b_{L/R}(2a^2_{L/R} + 1)}{2a^2_{L/R} + 2b^2_{L/R} - a_{L/R} b_{L/R} + 3},$$

$$a_R = q_{i+2} - q_{i+1}, \quad a_L = q_{i+1} - q_i, \quad b_R = q_{i+1} - q_i, \quad b_L = q_i - q_{i-1}.$$

Since the pressure is discretized using central differences, the scheme is stabilized following [Vier99] by a pressure diffusion of the form

$$F_{\mathbf{d}i+1/2,j} = \left(0,\, 0,\, 0,\, \eta \frac{p_{i+1,j} - p_{i,j}}{\beta_x}\right)^T, \qquad \beta_x = w_r + \frac{2\nu}{\Delta x}$$

where $T$ denotes transpose and $w_r$ is a reference velocity (in our case the maximum velocity in the flow field). Viscous fluxes are discretized using central differences on the dual mesh. This scheme is second-order accurate in space.

### *3.2 Time Integration*

The spatial discretization yields a system of ODE in the physical time $t$ variable, which is solved by the second-order BDF formula

$$P\frac{3W^{n+1}-4W^n+W^{n-1}}{2\Delta t}+\tilde{F}_x(W^{n+1})+\tilde{G}_y(W^{n+1})+\tilde{H}_z(W^{n+1})=\tilde{S}^{n+1}. \tag{8}$$

Here each tilde denotes a discrete approximation of $F_x, G_y, H_z, S$. Set

$$\begin{aligned} Res(W^{n+1},W^n,W^{n-1}) = P(&\frac{3}{2\Delta t}W^{n+1}-\frac{2}{\Delta t}W^n+\frac{1}{2\Delta t}W^{n-1})+\\ &+\tilde{F}_x(W^{n+1})+\tilde{G}_y(W^{n+1})+\tilde{H}_z(W^{n+1})-\tilde{S}^{n+1}. \end{aligned}$$

The above formula (8) is $Res(W,W^n,W^{n-1})=0$. It is solved by an artificial compressibility method in the dual time $\tau$. The system of equations

$$\tilde{P}W_\tau+Res(W,W^n,W^{n-1})=0$$

where $\tilde{P}=diag(1,1,1,1,\frac{1}{\beta^2})$, is solved by an explicit 3-stage second-order Runge–Kutta method.

## 4 Obstacle Modelling

We are interested in the solution of the stratified flows past a moving body. The obstacle is modelled very simply as a source term emulating a porous media with small permeability. This volume penalization technique was originally proposed by Arquis and Caltagirone [Cal84]. The source term $S(W)$ in this case is given by

$$\left[-v\frac{d\rho_0}{dz},0,0,-\rho g,0\right]^T+\frac{\chi(x,y,z,t)}{K}\left[0,U^{ob}-u,V^{ob}-v,W^{ob}-w,0\right]^T, \tag{9}$$

where $K$ corresponds to small permeability and $\chi(x,y,z,t)$ is the characteristic function of the obstacle, which moves with velocity $(U^{ob},V^{ob},W^{ob})$.

To estimate the influence of the permeability $K$, a very simple analytical model was developed. We suppose a 1D case, with the obstacle at rest and $U_0$ the velocity

of the incoming flow. The flow at the obstacle is decelerated only by the resistance of the body; other terms are omitted. This situation leads to

$$\dot{u} = -u/K, \qquad u(0) = U_0.$$

Integrating the velocity as $t \to \infty$, we obtain an estimate of the depth of penetration of fluid into the body:

$$u(t) = U_0 e^{-\frac{t}{K}} \quad \Rightarrow \quad s = \int_0^\infty u(t)dt = U_0 K.$$

If we prescribe the depth of penetration (this may be interpreted as the effective diameter of the obstacle), we can estimate the permeability $K$. For instance, in the case of a sphere of radius $r = 0.1\,\mathrm{m}$, a velocity $U_0 = 1\,\mathrm{m\,s^{-1}}$ and a penetration depth of 10% of $r$ lead to $K = s/U_0 = 1/100$.

## 5 Numerical Results

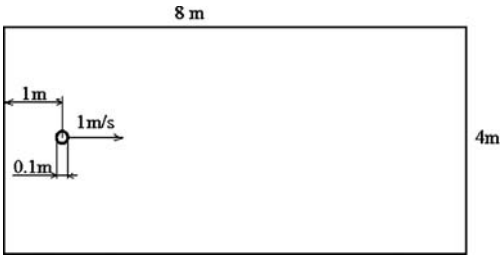


Towing tank

The obstacle is a sphere of radius 0.1 m, located 1 m from the left wall and at the midpoints of height and width see [Benes08]. At time $t = 0$ the obstacle starts moving to the right (in the positive $x$ direction) with constant velocity $U^{ob} = 1\,\mathrm{m\,s^{-1}}$. The flow field is initially at rest with stable density gradient $d\rho_0/dz = -0.1\,\mathrm{kg\,m^{-4}}$. The average density is $\rho_* = 1\,\mathrm{kg\,m^{-3}}$ and the kinematic viscosity is $\nu = 10^{-4}\,\mathrm{m^2\,s^{-1}}$. Homogeneous Dirichlet boundary conditions for the velocity and Neumann conditions for the density and pressure disturbances were used in 2D. In 3D, these boundary conditions were extended by periodic boundary conditions in the $y$-direction.

The problem was solved on Cartesian grids. In 3D, a mesh with $320 \times 40 \times 160$ cells was used. In 2D, a mesh with $320 \times 160$ nodes and, for testing of the mesh independence, a fine grid with $640 \times 320$ nodes were used.

Various stratification levels were modelled. To describe the stratification, the following bulk Richardson number is used:

$$Ri = \frac{g\frac{d\rho_0}{dz}}{\varrho_* U^{ob}}$$

For the numerical tests, the towing tank problem was used. The towing tank is a channel with the obstacle inside. Motion of this obstacle generates disturbances in the flow field. In the cases we solved, the towing tank has dimensions 8 m × 4 m in 2D or 8 m × 4 m × 1 m in 3D.

The degree of stratification is unaffected by changes in the density gradient, but by modifying the gravity constant in the range $g \in < 0, 1000 >$. The corresponding Richardson numbers satisfy $Ri \in < 0, 100 >$. The influence of permeability was also tested for selected values in range $K^{-1} \in < 0, 1000 > \mathrm{s}^{-1}$. The two numerical methods were compared.

Figures 1 and 2 compare the schemes in 2D. In the first figure we can see the comparison of density isolines at the time $t = 5\,\mathrm{s}$. The second figure displays the distribution of selected quantities in the transversal direction. These figures exhibit good agreement between both methods, especially further from the obstacle, while small differences occur behind the sphere. The maximal values predicted by WENO 5 scheme at the height midpoint are somewhat lower. Next, Fig. 3 examines

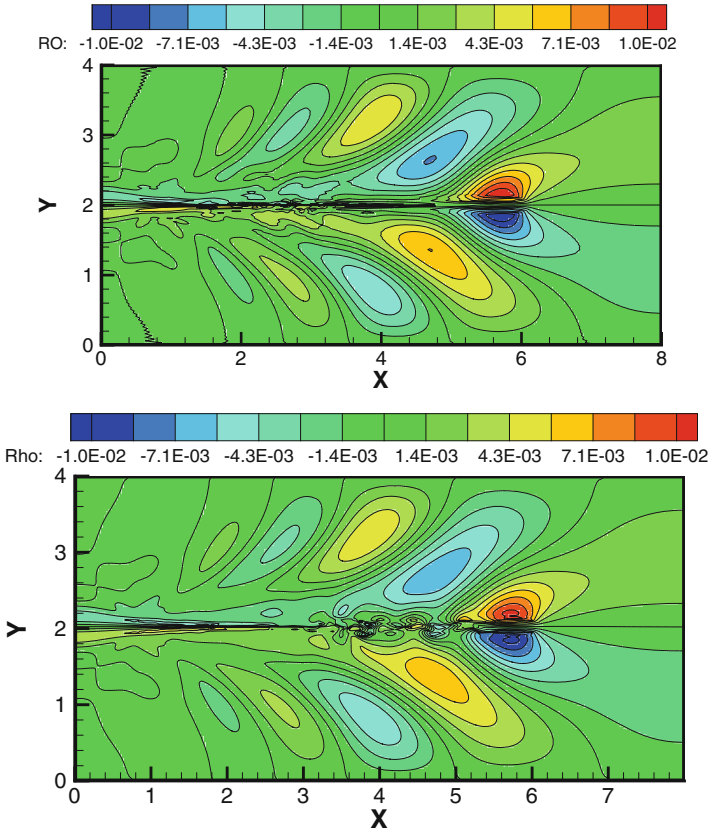


**Fig. 1** Comparison of isolines of the density disturbances for towing tank problem at the time $t = 5\,\mathrm{s}$, $g = 100$, $Ri = 10$. AUSM MUSCL scheme (*top*) and WENO5 (*bottom*)

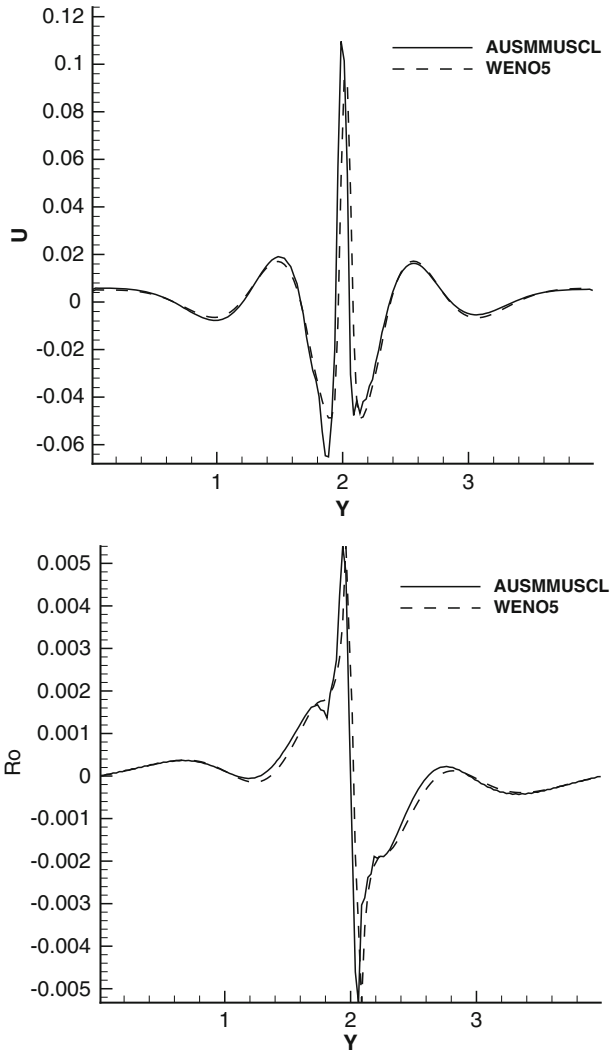


**Fig. 2** Comparison of both schemes, $Ri = 10$, time $t = 5$ s. Transversal distribution of the $u$-velocity component (*top*) and density disturbances (*bottom*), $y = 2.25$

the dependence of the solution on the mesh and shows that the solution is relatively mesh independent. Only the maxima of quantities at the height midpoint behind the obstacle are lower and they are probably not resolved correctly on this coarse mesh.

Figure 4 shows the dependence of the solution on the permeability $K$ for the three different values $1/K = 10, 100, 1000$. For the values 100 and 1,000 the solutions are very similar and the dependence on $K$ is low. The obstacle can be considered as impermeable for $1/K \geq 100$. The results are also in good agreement with the predictions given by our simple analytical model.

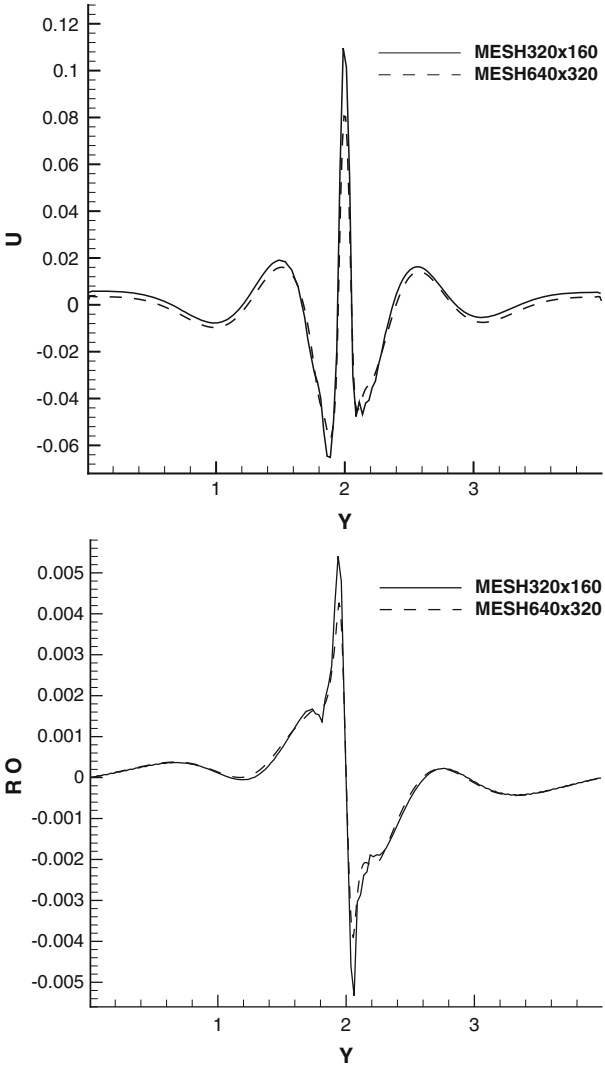


**Fig. 3** Dependence on the mesh, $Ri = 10$, time $t = 5$ s. Transversal distribution of the $u$-velocity component (*top*) and density disturbances (*bottom*), $x = 1$

Figure 5 displays the dependence of the flow on the Richardson number. A comparison of the isolines of density perturbation for four different Richardson numbers ($Ri = 0.1, 1, 10, 100$) is presented at the time $t = 6$ s. At a lower level of stratification behind the obstacle, a Karman vortex street forms. When the level of stratification increases, the character of the flow changes; wake instabilities are damped by stratification and internal gravity waves are clearly visible. Beyond this level, the obstacle generates a strip with constant density. The changes in the character of the flow are clearly visible in Fig. 6, where transversal distribution of

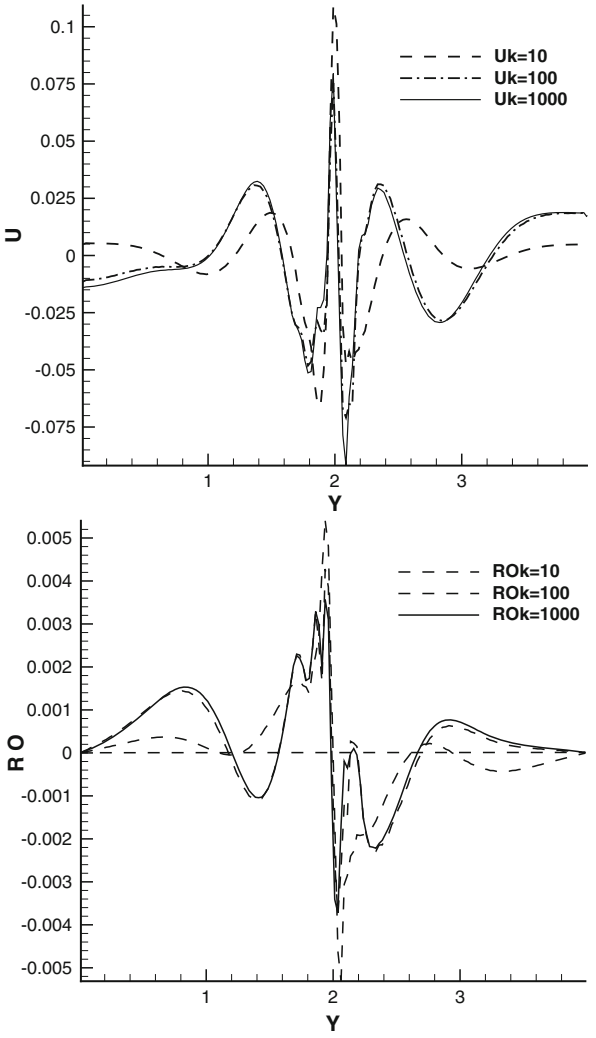


**Fig. 4** Dependence on the permeability parameter $K$, $Ri = 10$, time $t = 5$ s. Transversal distribution of the $\boldsymbol{u}$-velocity component (*top*) and density disturbances (*bottom*), $x = 1$

computed quantities for different Richardson numbers are shown. For comparison see [Ber01].

The isosurfaces of the vorticity in 3D for the Richardson numbers $Ri = 1$ and $Ri = 10$ are shown in Fig. 7. The marked influence of stratification can be seen at the $x$–$z$ cross-section. In the case $Ri = 1$, the influence of stratification is small and the shape of vorticity in the cross-section is close to a circle. On the other hand, for the higher level of stratification $Ri = 10$ the vortices are damped differently in different directions, which leads to an asymmetry in the vorticity isosurface.

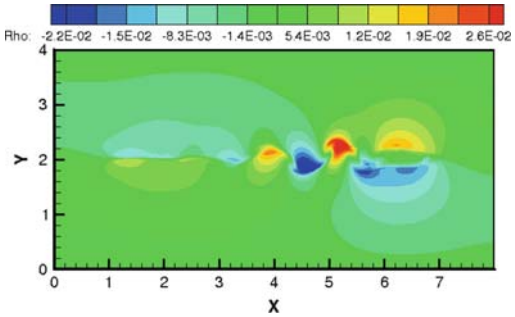


(a) $Ri = 0.1$

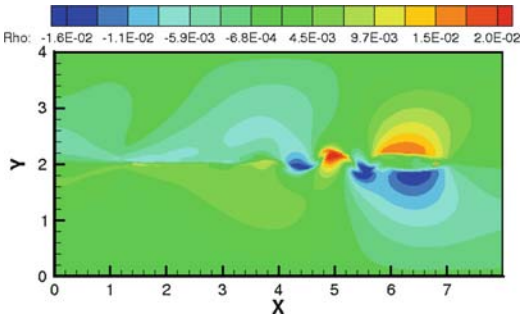


(b) $Ri = 1$

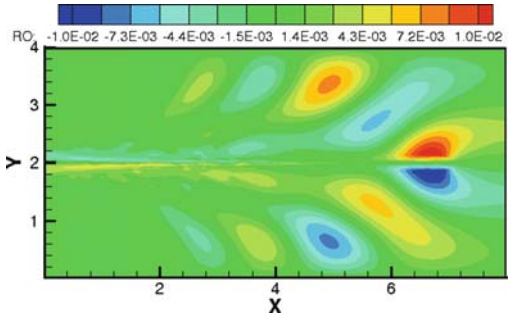


(c) $Ri = 10$

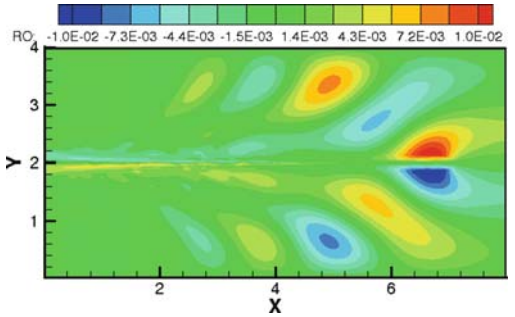


(d) $Ri = 100$

**Fig. 5** Isolines of density perturbations for different values of $Ri$. Time $t = 6$ s

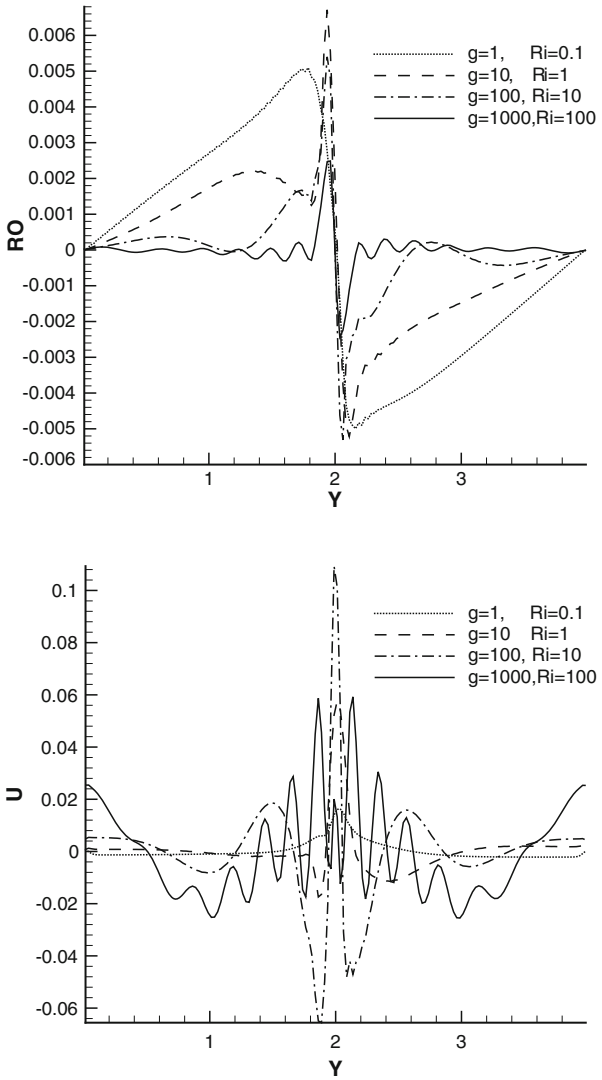


**Fig. 6** Transversal distribution of density disturbances (*top*) and $u$-velocity component (*bottom*) for different Richardson numbers, $x = 1$, time $t = 6$ s

The isosurfaces of the density perturbations in 3D for the same Richardson numbers are shown in Fig. 8. The internal gravity waves with Brunt–Väisälä frequency are clearly visible.

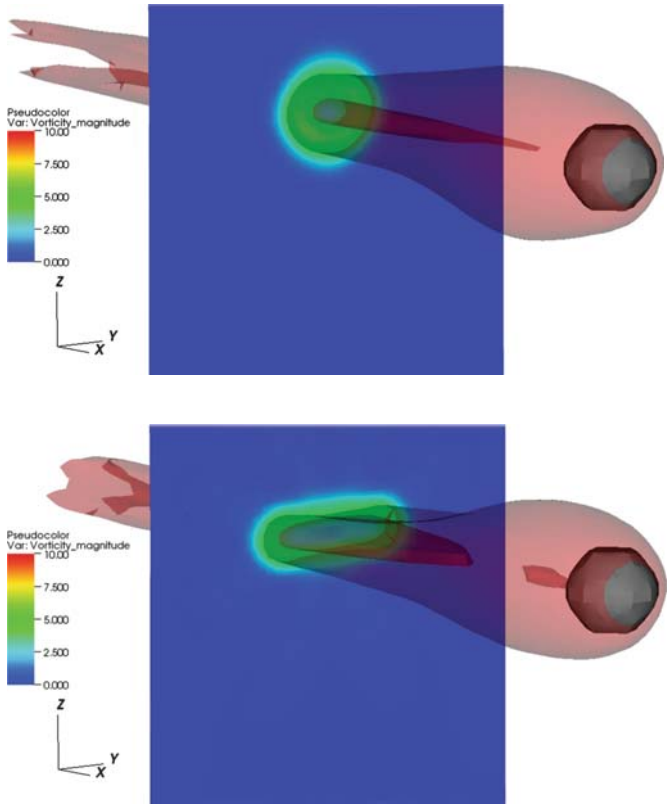


**Fig. 7** Vorticity distribution for the Richardson numbers $Ri = 1$ (*top*) and $Ri = 10$ (*bottom*), time $t = 5$ s

## 6 Conclusion

Two numerical methods for simulation of 2D and 3D stratified flows have been developed. Such simulations are necessary for more complicated situations, where experimental data or other information about solution is no longer available. Since the solution can depend on the numerical scheme, a comparison of solutions obtained using different methods eliminates this dependence. Both methods have been used successfully for the towing tank problem. The numerical results obtained are in good mutual agreement and also match physical expectations.

Numerical results were obtained for Richardson numbers $Ri \in < 0, 100 >$ and permeability $K \in < 1, 1000 >$. From this, according to our simple analytical model, it follows that the minimal value of permeability is $K \geq 100$. The dependence of the solution on the mesh was also tested. The computations performed demonstrate the applicability of our methods to the simulations of stratified flows.

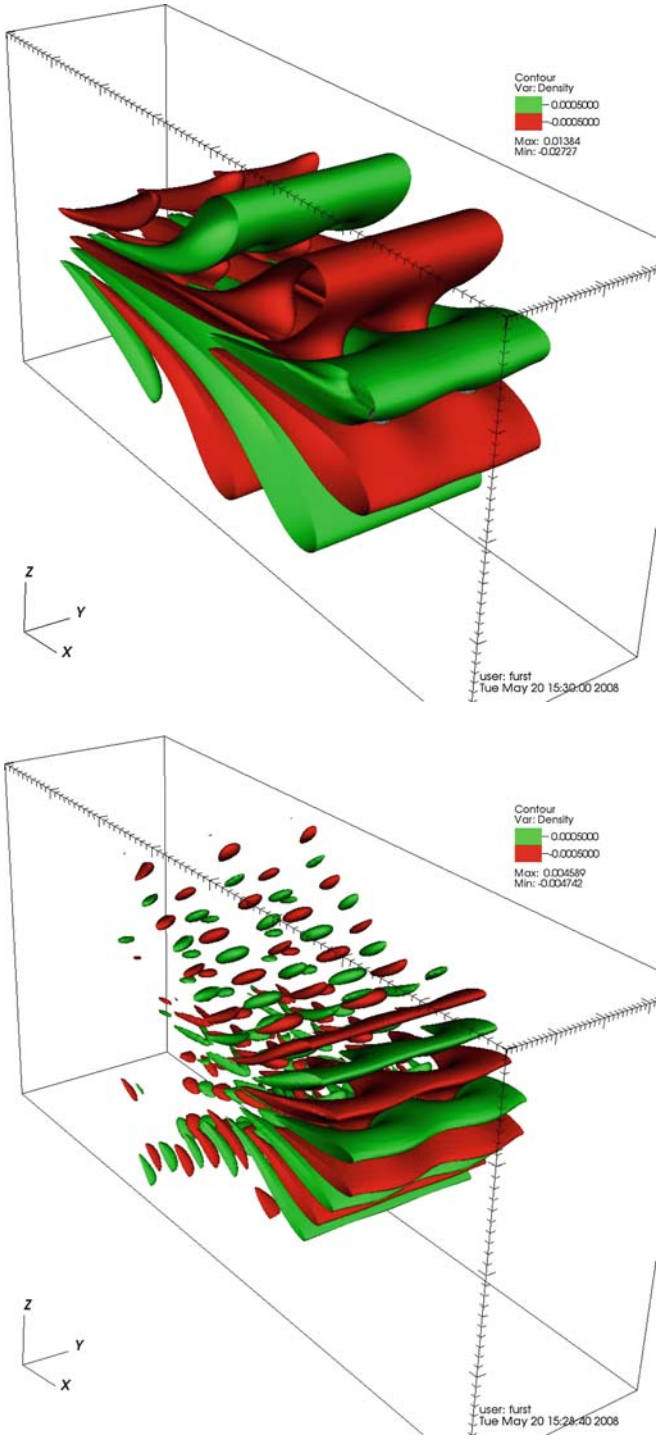


**Fig. 8** Isosurfaces of the density perturbations at the time $t = 5$ s; $Ri = 10$ on *top*, $Ri = 100$ on *bottom*

An open question is the choice of appropriate boundary conditions; those used in the current approach are suitable for the simulation of flows in a domain bounded with walls. Alternative conditions should be considered for free atmosphere flows.

**Acknowledgements** This work was supported by Research Plan MSM 6840770003, by GACR Project No.205/06/0727 and by grant GA 201/08/0012.

## References

[Cal84] Arquis E., Caltagirone J.P.: Sur les conditions hydrodynamiques au voisinage dune interface milieu fluide milieu poreux: application a la convection naturelle. C.R. Acad. Sci. Paris II **299**, 1–4 (1984)

[Bla01] Blazek J.: Computational Fluid Dynamics: Principles and Applications. Elsevier Science, Amsterdam, 2001, ISBN 0080430090

[Ber01] Berrabaa S., Fraunie P.H., Crochet M.: 2D large eddy simulation of highly stratified flows: the stepwise structure effect. Advances in Computation. Scientific Computing and Applications, volume 7. Nova, Hauppauge, NY, 2001, pp. 179–185

[Jiang96] Chi-Wang Shu, Guang-Shan Jiang: Efficient implementation of weighted eno schemes. J. Comput. Phys. **126**, 202–228 (1996)

[Furst96] Kozel K., Angot Ph., Fürst J.: TVD and ENO schemes for multidimensional steady and unsteady flows. In: Benkhaldoun F., Vilsmeier R. (eds) Finite Volumes for Complex Applications. Hermes, Paris, 1996, pp. 283–290

[Vier99] Dick E., Vierendeels J., Riemslagh K.: A multigrid semi-implicit line-method for viscous incompressible and low-mach-number flows on high aspects ratio grids. J. Comput. Phys. **154**, 310–341 (1999)

[Issa85] Issa R.I.: Solution of the implicitly discretized fluid flow equations by operator-splitting. J. Comput. Phys. **62**, 40–65 (1985)

[Benes08] Fraunie Ph., Beneš L., Fürst J.: Numerical simulation of the stratified flow. In: Proceeding of conference Topical Problems of Fluid Mechanics 2008, 5–8 (2008)